

# Exposing Synthetic Speech: Model Attribution and Detection of AI-generated Speech via Audio Fingerprints

Matías Pizarro<sup>1</sup> Mike Laszkiewicz<sup>1</sup> Shawkat Hess<sup>1</sup> Dorothea Kolossa<sup>2</sup> Asja Fischer<sup>1</sup>

<sup>1</sup>*Faculty of Computer Science, Ruhr University Bochum, Germany*

<sup>2</sup>*Electronic Systems of Medical Engineering, Technische Universität Berlin, Germany*

**Abstract**—As speech generation technologies continue to advance in quality and accessibility, the risk of malicious use cases, including impersonation, misinformation, and spoofing, increases rapidly. This work addresses this threat by introducing a simple, training-free, yet effective approach for detecting AI-generated speech and attributing it to its source model. Specifically, we tackle three key tasks: (1) single-model attribution in an open-world setting, where the goal is to determine whether a given audio sample was generated by a specific target neural speech synthesis system (with access only to data from that system); (2) multi-model attribution in a closed-world setting, where the objective is to identify the generating system from a known pool of candidates; and last but not least (3) detection of synthetic versus real speech. Our approach leverages standardized average residuals—the difference between an input audio signal and its filtered version using either a low-pass filter or the EnCodec audio autoencoder. We demonstrate that these residuals consistently capture artifacts introduced by diverse speech synthesis systems, serving as distinctive, model-agnostic fingerprints for attribution. Across extensive experiments, our approach achieves AUROC scores exceeding 99% in most scenarios, evaluated on augmented benchmark datasets that pair real speech with synthetic audio generated by multiple synthesis systems. In addition, our robustness analysis underscores the method’s ability to maintain high performance even in the presence of moderate additive noise. Due to its simplicity, efficiency, and strong generalization across speech synthesis systems and languages, this technique offers a practical tool for digital forensics and security applications.

**Index Terms**—synthetic speech detection, model attribution, digital forensics, residual fingerprints, neural synthesis systems

## 1. Introduction

With the rapid advancement of synthetic data generation technologies, distinguishing between genuine and artificial speech signals has become increasingly challenging. This issue is particularly relevant today because public and open-source tools enable even unskilled attackers to synthesize highly realistic voice samples that closely resemble human speech [1], [2]. Although these technologies offer

numerous advantages, such as improving accessibility for speech-impaired individuals [3] and supporting multilingual communication [4], they also pose several security risks. Most pressingly, synthetic speech poses a growing threat to security by enabling spoofing attacks on Automatic Speaker Verification (ASV) systems, as well as impersonation and circumvention of other voice-controlled systems. These threats can be exploited in various harmful ways, such as disinformation campaigns [5], biometric spoofing attacks [6], misleading juries in criminal trials through forged audio evidence [7], or cloning voices to commit identity fraud [8], [9].

The emergence of synthetic audio as a vector for impersonation and manipulation presents a direct challenge to the security and trustworthiness of modern communication systems. While deepfake detection models offer a line of defense, many require costly supervised training and large labeled datasets—limiting their scalability. This highlights the need for more lightweight or training-free attribution methods. Given the risks of synthetic speech signals, various countermeasures have been proposed, focusing primarily on binary deepfake detection. This objective is reflected in several well-established benchmark challenges such as Automatic Speaker Verification Spoofing (ASVspoof) [10] and Audio Deepfake Detection (ADD) [11]. However, an essential gap remains: *model attribution*, also known as *algorithm recognition*, that is, the identification of the specific data-generating model behind a synthetic speech signal, is still underexplored.

This attribution plays a vital role in real-world forensics and security analysis, where linking synthetic speech to its source model can aid in identifying malicious actors, tracing the origin of disinformation campaigns, enforcing intellectual property rights, and strengthening cybersecurity threat analysis. Recent studies have explored multiclass classification approaches to attribute speech samples to specific synthesis systems. However, these models operate in a closed-world setting [12], [13], which means that they can only recognize systems seen during training. As a result, they do not generalize to new models without costly retraining, which presents a major limitation given the rapid evolution of synthetic speech technologies.

This paper presents a novel, efficient, and training-free approach to speech synthesis system attribution as well as

synthesized speech detection that can be directly applied to cybersecurity and forensic workflows. To the best of our knowledge, we introduce the first single-model attribution technique in an open-world setting, i.e., a technique allowing to identify whether a speech sample was generated by a specific model while distinguishing it from any unseen speech synthesis systems or even from real speech. Notably, our method only requires samples from *one* target model and does not require training a costly machine learning classifier, making it highly adaptable to newly evolving synthetic speech technologies. In addition to open-world attribution, our method represents an easy and cheap approach to closed-world model classification and synthetic speech detection. Therefore, our method provides a unified solution to multiple threat scenarios, and notably, it outperforms state-of-the-art strategies in all these settings. Precisely, our key contributions are as follows:

- 1) Discovery of model-specific speech fingerprints: We demonstrate that neural speech synthesis systems leave behind consistent, model-specific artifacts in generated audio. These subtle residual patterns act as reliable fingerprints and persist across diverse samples.
- 2) Proposal of a unified attribution and detection framework: We propose a lightweight, training-free method that exploits these fingerprints to perform both model attribution (in single- and multi-model settings) and synthetic speech detection.
- 3) Extensive empirical evaluation: We evaluate our technique on a broad variety of datasets and speech generation systems and demonstrate its robustness to real-world noise. Our approach remains effective under moderate background noise, highlighting its suitability for forensic and security applications in realistic, uncontrolled environments.

By addressing the attribution and detection of synthetic speech as a response to malicious misuse of generative models, this work advances the development of lightweight, deployable defenses against speech synthesis attacks, contributing directly to applied cybersecurity.

## 2. Problem Setup and Thread Models

The rise of advanced speech synthesis models—both text-to-speech (TTS) [14] and voice conversion (VC) [15]—poses a significant threat to the integrity and trustworthiness of modern communication systems. These models can be used to impersonate individuals, generate persuasive misinformation, and compromise authentication systems. TTS systems generate speech from arbitrary text inputs using a target speaker’s voice, while VC systems modify a source speaker’s voice to resemble a target speaker’s voice, preserving the linguistic content.

From a security and forensic perspective, it is critical to develop techniques that can reliably detect AI-generated audio. But detection alone is not sufficient. It is also of great relevance to be able to attribute synthetic audio to its generative source. This enables defenders to (1) trace

the origin of misinformation or impersonation attacks, (2) hold the creators of malicious content accountable, and (3) design targeted countermeasures against specific synthesis models—for example, in high-security environments (like banking voice authentication or governmental communications), systems might deploy lightweight model-specific classifiers to flag suspicious audio in real-time, apply adaptive thresholds based on the known behavior of the synthesis model, or use the model’s outputs to adversarially train more robust detection systems. It is also of importance from the perspective of the model owner, since it can be employed to detect model theft or the illegal usage of a model.

**Attacker model:** We assume a non-adaptive adversary with access to one or more generative speech models. These may be public (e.g., open-source) or proprietary systems, and the attacker can generate synthetic audio, which is transmitted losslessly to the target system. The adversary does not know which detection or attribution mechanism will be used by the defender.

**Defender model:** The defender aims to detect or attribute potentially fake audio samples. Their capabilities vary across scenarios—ranging from having access to generated data from only one synthesis model to having data from multiple generators. Attribution relies on the audio samples alone, without knowledge of the internal workings of the generative models.

### 2.1. Problem Settings

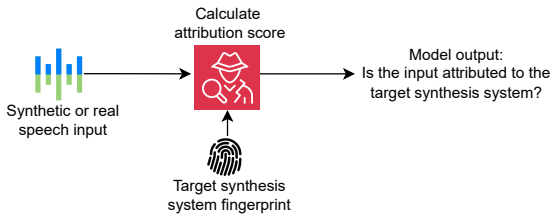
We define the attribution problem along two dimensions:

- Single-model vs. multi-model: Data of how many synthesis models is available to the defender for constructing the attribution technique?
- Open-world vs. closed-world: Is the synthesis model used by the attacker assumed to be included in the construction phase of the attribution method, or can it be a previously unseen (unknown) model?

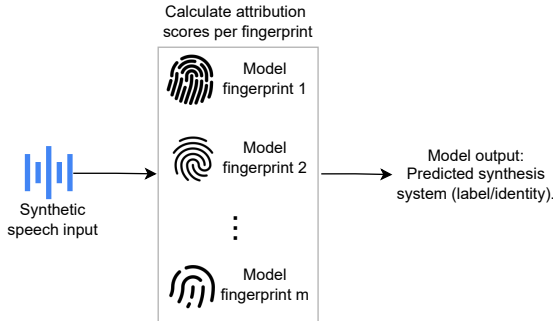
These axes define three core scenarios illustrated in Fig. 1 and detailed below.

**Single-Model Attribution in an Open-World Setting (Fig. 1a).** In this scenario, the defender has training data from only one known synthesis model and wants to detect whether a given audio sample—potentially real, or generated by an unknown system—was synthesized by this specific model. This setting is relevant in scenarios such as a model owner seeking to determine whether their proprietary synthesis model has been misused or leaked, or in cases where monitoring is needed for the misuse of a specific model known to be high-risk. It represents a challenging and underexplored problem that demands generalization to unseen distributions, potentially across different languages or speakers.

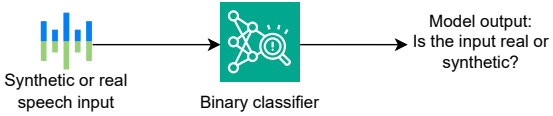
**Multi-Model Attribution in a Closed-World Setting (Fig. 1b).** Here, the defender has access to samples from several synthesis models when constructing the attribution



(a) **Single-Model Attribution in an Open-World Setting:** Detects whether an audio, which could be synthetic or real, has been generated by a specific target speech synthesis system.



(b) **Multi-Model Attribution in a Closed-World Setting:** Classifies the synthetic audio as originating from one of several known models.



(c) **Real vs. Synthetic Detection:** Classifies whether the input is genuine human speech or synthetic.

Figure 1: Illustration of the architecture of our audio fingerprinting system designed for synthetic audio detection and attribution in operational security contexts. The system ingests audio input and routes it through three complementary modules, each serving a distinct detection purpose: (a) single-model attribution in an open-world setting, (b) multi-model attribution in a closed-world setting, and (c) real vs. synthetic detection. These components may be deployed independently or in sequence depending on the application, such as forensic voice analysis, authentication integrity checks, or deepfake detection at content platforms.

technique, and all models encountered at test time are among those known. The goal is to correctly classify which model generated the synthetic input. This setting assumes that all relevant generative models have been observed beforehand and is common in prior work [12], [13], [16], [17]. Applications include forensic tracing where the defender wants to narrow down the toolchain used by an attacker among a known set of synthesis technologies.

**Real vs. Synthetic Detection (Fig. 1c).** This is the classic deepfake detection task: determining whether an input is human or machine-generated. This task is well studied [10], often using supervised or contrastive learning with training data from a range of synthesis models. It usually relies on training machine learning classifiers that are trained to distinguish generated data (from multiple generative models) from real audio samples, and thus can be situated in the multi-model, closed-world setting.

## 2.2. Threat Scenarios in Practice

Each setting corresponds to practical applications with varying levels of difficulty and generalization requirements:

- (a) **Single-Model Attribution in an Open-World Setting:** Critical for model owners, IP protection, and threat monitoring of specific high-risk tools—despite the limited training data.
- (b) **Multi-Model Attribution in a Closed-World Setting:** Useful for law enforcement or forensic analysts who can obtain samples from all suspected models.
- (c) **Real vs. Synthetic Detection:** Widely used in spoofing detection and authentication systems.

## 3. Related Work

This section reviews existing research on the detection and attribution of synthetic audio—commonly known as audio deepfake detection—focusing on approaches suitable for practical, automated identification of generative model outputs. It also revisits the concept of generative model fingerprints, originally proposed in the computer vision domain for generative adversarial networks (GANs).

### 3.1. Deepfake Detection Approaches

Research in deepfake detection spans anti-spoofing techniques and synthesis system attribution methods.

**3.1.1. Spoofing Detection Systems.** These systems typically consist of an acoustic feature extractor and a classifier. The acoustic feature extractor is designed to extract relevant characteristics from the raw audio input, which are then forwarded to the classifier. Examples of spectral features include Linear-Frequency Cepstral Coefficients (LFCC) [18], Mel-Frequency Cepstral Coefficients (MFCC) [18], Constant Q Cepstral Coefficients [19], and long-term variable Q transform [20]. The classifier is then trained on these acoustic features to distinguish real from synthetic audio samples.

Classifier models that have demonstrated effectiveness for this task are based on Gaussian mixture models [21] or various types of neural networks like X-vector [22], Light Convolutional Neural Networks (LCNNs) [23], [24], Residual Networks (ResNets) [25]–[27], Squeeze-Excitation and Residual Networks (SE-ResNets) [28]–[30], Graph Attention Networks [31], [32], Differentiable Architecture Search [33], and Transformers [34].

**3.1.2. Synthesis System Attribution Methods.** In contrast, model attribution aims to identify the specific generative synthesis system responsible for producing the synthetic audio samples. Deep learning-based synthesis systems outperform traditional parametric and concatenative methods in both speech quality and flexibility, leveraging neural networks to generate high-fidelity speech with improved prosody and speaker similarity.

Among the most successful synthesis system approaches are GAN-based models [16], which leverage adversarial training to generate high-quality, low-latency speech; Flow-based models [35], which utilize invertible transformations for efficient waveform synthesis; Diffusion-based models [36], which refine noise into speech through iterative processes, achieving state-of-the-art quality at the cost of higher computational requirements; and Hybrid signal processing-deep learning models [37], which combine traditional signal processing techniques with deep learning to improve interpretability and control in speech synthesis.

Frank and Schönherr [16] observed that speech generated by GAN-based synthesis systems exhibits artifacts, particularly in the higher frequency ranges, that are characteristic of the underlying generation method. Yan et al. [12] utilized LFCC features and a ResNet classifier to detect audio produced by eight different synthetic speech models, while Li et al. [17] applied MFCCs and a lightweight CNN to classify samples generated by four such systems. Similarly, Deng et al. [13] employed Mel spectrograms and trained a neural network using contrastive learning to identify synthetic speech generated by six distinct models.

## 3.2. Limitations of Prior Work

Prior efforts, while effective in closed-world settings, struggle with generalization to unknown generative models, often due to overfitting or limited training diversity. An example of recent work addressing this limitation is the third track of the ADD 2023 challenge [11], which includes an open-world model attribution task. However, it differs from our approach in three key ways. First, the attribution techniques were evaluated based on data from 8 different sources, from which 7 were known during training. The existence of multiple models during training allows to leverage latent representations of a trained classifier, as deployed by the winner of the challenge [38], or to make use of contrastive learning, as deployed by the runner-up [39]. In the single-model setting, that is, when restricting access to data from only a single source during training, these techniques are not applicable. Secondly, the evaluation in ADD puts more emphasis on the closed-world performance as the dataset contains around  $7/8 = 87.5\%$  samples from generative models seen during training. Lastly, the dataset utilized in ADD is not publicly available, which limits its reproducibility significantly.<sup>1</sup> In contrast, this paper emphasizes the open-world attribution task while also considering

<sup>1</sup> The dataset cannot be reproduced because the source of the unknown class is not shared.

the closed-world setting, supporting practical use in cybersecurity operations such as fake audio detection and attribution of generative model sources.

In parallel, fake speech prevention has emerged as a proactive line of defense, aiming to stop unauthorized synthesis before it occurs. For instance, this can be achieved by introducing subtle perturbations to a target speaker’s audio before it is accessed by an attacker [40], or by altering the audio in the frequency domain prior to sharing or distribution [41]. While such approaches are effective in protecting user privacy and mitigating synthesis attacks, they differ fundamentally from model attribution. Prevention techniques aim to block the synthesis process, whereas model attribution seeks to identify the specific system responsible for already generated synthetic audio. As such, attribution complements both prevention and detection strategies by enabling post-hoc forensic and investigative capabilities.

## 3.3. Revisiting GAN Fingerprints

The concept of model-specific fingerprints was initially explored by Marra et al. [42] in the context of image generation using GANs. Their idea is based on the assumption that any artificially generated image  $x$  decomposes into its content  $I(x)$  and a fingerprint  $F$  that is unrelated to the image semantics but specific to the model, that is,  $x = I(x) + F$  for every  $x$  generated from the model. To extract the fingerprint, they assumed that a suitable image filter  $f$  is capable of removing the fingerprint, such that  $f(x) \approx I(x)$ , and therefore  $R := x - f(x) \approx F$ . Given a set of generated samples  $x_1, \dots, x_N$ , the sample-wise residuals are defined by  $R_i := x_i - f(x_i)$  and  $\hat{F}$  is estimated by  $\hat{F} := \frac{1}{N} \sum_{i=1}^N R_i$ . For inference, i.e., for checking whether a test sample  $x_{\text{test}}$  contains a fingerprint similar to  $\hat{F}$ , they first compute its residual  $R_{\text{test}}$  as above and then assign the correlation score  $s_{\text{cor}}(x_{\text{test}}; \hat{F}) := \langle \tilde{R}_{\text{test}}, \hat{F} \rangle \in [-1, 1]$ , where  $\tilde{R}_{\text{test}}$  and  $\hat{F}$  denote the zero-mean and unit-norm versions of  $R_{\text{test}}$  and  $\hat{F}$ , respectively. Having a set of  $m$  different generative models, and therefore, a set of corresponding fingerprints  $\hat{F}_1, \dots, \hat{F}_m$ , one attributes a sample to the  $j$ th model, where  $j = \arg \max_{i \in [m]} s_{\text{cor}}(x_{\text{test}}; \hat{F}_i)$ .

## 4. Methodology

We propose an audio fingerprinting methodology for model attribution, inspired by approaches developed for GAN-generated images, which is largely unexplored in the audio domain. Unlike images, audio signals pose unique challenges for fingerprint extraction. This task presents two main challenges that distinguish audio fingerprinting from its image counterpart:

- 1) **Variable-length:** Unlike fixed-size images, audio signals vary in duration, but fingerprint extraction requires a fixed-size representation for consistent analysis.
- 2) **Content-preserving filtering:** While image fingerprints rely on spatial filtering, audio requires filters that suppress content-related features such as speech seman-

tics and phonetics, while preserving subtle generative model-specific artifacts.

Our pipeline addresses these challenges by first converting each audio sample to an average spectral energy representation and then applying suitable filters to extract residuals, which are averaged to form a fingerprint as detailed in the following.

## 4.1. Average Energy Representation

To overcome the length variability of the audio signals, we transform each signal into a fixed-size representation that summarizes its spectral content. We apply the Short-Time Fourier Transform (STFT), which converts a time-domain signal into a time-frequency representation known as a spectrogram.

First, let  $x^{(i)}$  be a discrete-time audio signal of arbitrary length, representing the  $i$ -th sample. Since the frequency content of audio signals typically changes over time, applying a single global Fourier Transform would only provide an average frequency representation over the entire signal, thereby losing important temporal information. To capture how the frequency components evolve, we divide the signal into overlapping short-time frames  $x^{(i)}(k, t)$ , where:

- $k \in \{0, \dots, L-1\}$  is the time index within each frame of length  $L$  (i.e., there are  $L$  discrete amplitude values per frame),
- $t \in \{1, \dots, T^{(i)}\}$  is the frame index, where  $T^{(i)}$  is the total number of frames obtained by sliding a window over signal  $x^{(i)}$ .

Frames are often overlapped (e.g., 25% overlap) to improve temporal continuity and reduce artifacts from abrupt frame boundaries. Therefore, the total number of frames  $T^{(i)}$  depends on the signal length, the sampling rate, the frame length  $L$ , and the hop size (i.e., the number of samples between consecutive frames).

Second, to mitigate spectral leakage at frame boundaries, each frame is multiplied by a smooth window function  $\omega(k)$ , such as a Hann or Hamming window:

$$x_{\omega}^{(i)}(k, t) = x^{(i)}(k, t) \cdot \omega(k) .$$

This smooths the signal at the boundaries of each frame before applying the Fourier Transform. We then apply the Discrete Fourier Transform to each windowed frame:

$$X_{\text{DFT}}^{(i)}(f, t) = \sum_{k=0}^{L-1} x_{\omega}^{(i)}(k, t) \cdot e^{-j2\pi kf/L} ,$$

where  $f \in \{0, \dots, L-1\}$  is the frequency bin index, and  $X_{\text{DFT}}^{(i)}(f, t) \in \mathbb{C}$  is the complex frequency spectrum of frame  $t$ . To obtain the spectrogram, we take the magnitude of the complex spectrum:

$$S_X^{(i)}(f, t) = \left| X_{\text{DFT}}^{(i)}(f, t) \right| .$$

The resulting spectrogram  $S_X^{(i)} \in \mathbb{R}^{F \times T^{(i)}}$  represents the signal’s energy distribution over time and frequency, where

$F$  is the number of unique frequency bins. We apply a logarithmic transformation to map power values to decibels:

$$\mathcal{S}_X^{(i)}(f, t) = 10 \cdot \log_{10} \left( S_X^{(i)}(f, t) \right) .$$

To obtain a fixed-size representation independent of audio length, we compute the average energy per frequency bin:

$$E_{x^{(i)}}[f] := \frac{1}{T^{(i)}} \sum_{t=1}^{T^{(i)}} \mathcal{S}_X^{(i)}(f, t) ,$$

yielding a vector  $E_{x^{(i)}} \in \mathbb{R}^F$  that summarizes the spectral energy distribution across time. This time-frequency representation forms the basis for our subsequent fingerprint estimation method that requires a fixed-size input.

## 4.2. Suitable Filtering Methods

To isolate generative artifacts, we apply content-preserving filters to the audio signal before computing the residuals of our spectral energy representation. We investigate two types of filtering approaches: (1) neural compression using EnCodec, and (2) spectral filtering, including low-pass, high-pass, band-stop, and band-pass filters.

**EnCodec** [43]. EnCodec is a neural audio compression model based on a quantized latent representation. We use a pre-trained causal model operating at 24 kHz on monophonic audio, trained on a variety of audio data.<sup>2</sup> It consists of:

- An encoder that transforms the input waveform into a latent vector  $\mathbf{w}$ ,
- A quantizer that maps  $\mathbf{w}$  to a discretized version  $\mathbf{w}_q$ ,
- A decoder that reconstructs the waveform from  $\mathbf{w}_q$ .

This architecture preserves the overall content while discarding fine-grained details, making it suitable for suppressing speech synthesis-specific artifacts.

**Spectral Filtering.** As an alternative to neural compression, we apply finite impulse response (FIR) filtering to manipulate the spectral characteristics of the audio signal in a controlled and interpretable manner. By selectively preserving or attenuating different frequency bands—such as low, high, or mid frequencies—we aim to suppress content-related information while retaining generative artifacts introduced by the synthesis model.

An FIR filter operates by convolving the input signal with a set of learned or designed filter coefficients. Given a discrete-time input signal  $x^{(i)} = \{x_1^{(i)}, x_2^{(i)}, \dots, x_s^{(i)}\}$ , the filtered output  $y^{(i)} = \{y_1^{(i)}, y_2^{(i)}, \dots, y_s^{(i)}\}$  is obtained via convolution:

$$y_n^{(i)} = \sum_{k=0}^{K-1} h_k \cdot x_{n-k}^{(i)}, \quad \text{for } n = 1, \dots, s ,$$

2. <https://github.com/facebookresearch/encodec>.

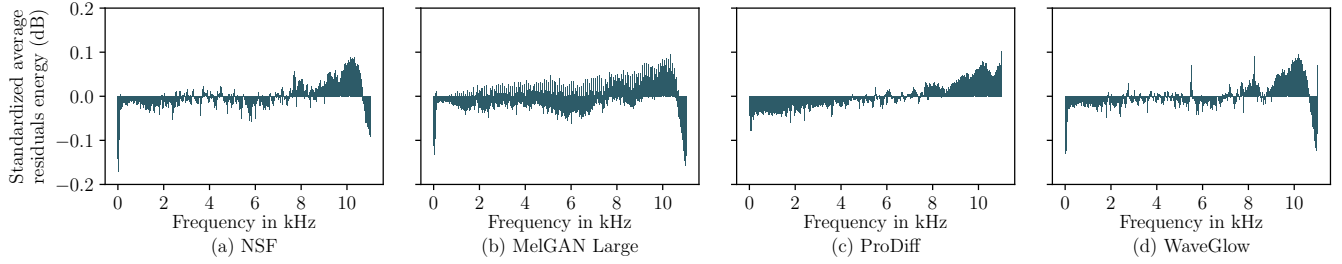


Figure 2: Extracted fingerprints  $\hat{\mathcal{F}}$  from four speech synthesis systems, computed as the average residuals (Equation 1) between the average spectral energy  $E_{x^{(i)}}$  of generated audio samples and their EnCodec-filtered counterparts  $E_{f(x^{(i)})}$ , highlighting model-specific spectral characteristics.

where  $h_k$  are the filter coefficients, and  $K$  is the filter order, i.e., the number of coefficients in the FIR filter. Zero-padding is applied when  $n - k < 1$ . This corresponds to a standard 1D convolution operation with one input and one output channel. By choosing appropriate coefficients, we can implement low-pass, high-pass, band-stop, or band-pass behavior depending on which frequency bands we aim to isolate or suppress. This enables a flexible residual extraction strategy that highlights synthesis-specific artifacts while reducing the influence of linguistic content and speaker identity.

### 4.3. Fingerprint Extraction

Given a set of  $N$  audio signals  $\{x^{(i)}\}_{i=1}^N$ , we estimate the generative model’s fingerprint  $\hat{\mathcal{F}}$  by averaging the residuals between the original and filtered average energy representations:

$$\hat{\mathcal{F}} := \frac{1}{N} \sum_{i=1}^N \mathcal{R}^{(i)}, \quad \text{where } \mathcal{R}^{(i)} := E_{x^{(i)}} - E_{f(x^{(i)})}. \quad (1)$$

Here,  $f(\cdot)$  denotes the chosen filter (e.g., EnCodec or spectral filtering), and  $\mathcal{R}^{(i)} \in \mathbb{R}^F$  is the residual vector for signal  $x^{(i)}$ . Figure 2 exemplarily illustrates the EnCodec-based fingerprints for four different speech synthesis systems. Each fingerprint represents the standardized average residual energy distribution across frequencies, computed from the residual spectrograms. As seen in the figure, the fingerprints exhibit distinct patterns, highlighting that different synthesis systems leave characteristic traces in the frequency domain. These differences form the basis for discriminating among models in attribution tasks.

### 4.4. Scoring and Attribution

As an alternative to the correlation-based scoring method  $s_{\text{cor}}$  defined in Section 3.3, we propose a scoring method based on the Mahalanobis distance, which accounts for correlations between features. Given a test sample  $x_{\text{test}}$ , we compare its residual vector  $\mathcal{R}_{\text{test}}$  to the fingerprint  $\hat{\mathcal{F}}$  via:

$$s_{\text{md}}(\mathcal{R}_{\text{test}}, \hat{\mathcal{F}}) := \sqrt{(\mathcal{R}_{\text{test}} - \hat{\mathcal{F}})^\top \Sigma^{-1} (\mathcal{R}_{\text{test}} - \hat{\mathcal{F}})},$$

where  $\Sigma^{-1}$  is the inverse covariance matrix of the training residuals. This distance accounts for feature variance and correlation, enabling more robust attribution. It has proven effective in tasks like out-of-domain detection [44], [45].

**Attribution Criteria.** While the correlation score measures the alignment between a test residual and a fingerprint—where higher values indicate stronger attribution—the Mahalanobis distance is defined such that lower distances imply higher similarity. Thus, for attribution, we can either *maximize*  $s_{\text{cor}}$  to assign  $x_{\text{test}}$  to the closest fingerprint in terms of Pearson correlation, or *minimize*  $s_{\text{md}}$  to assign  $x_{\text{test}}$  to the closest fingerprint in terms of Mahalanobis distance.

## 5. Evaluation and Results

All experiments are conducted using publicly available speech synthesis systems and benchmark baselines. Each experiment is repeated five times to ensure statistical reliability, and we report the average results across runs. In all cases, the test sets consist of unseen real and synthetic samples to reliably assess generalization performance. The code, pre-trained models, filter coefficients, and synthetic audio samples used in our experiments are available at <https://github.com/blindconf/fingerprint>.

### 5.1. Datasets

To ensure a comprehensive evaluation of our attribution method across diverse synthesis techniques and deployment scenarios, we utilize multiple speech corpora and include synthetic speech generated by a wide range of systems. This setup allows us to assess model attribution performance under various architectural paradigms, and to evaluate generalization across different speakers, languages, and domains. We focus primarily on three datasets:

**Augmented LJSpeech Benchmark (English).** We use the LJSpeech corpus [46], a single-speaker English dataset comprising 13,100 audio clips. Synthetic speech samples for this dataset are drawn from the WaveFake dataset [16] and its extension [47], which cover a wide range of speech synthesis

systems. In addition, we augment the dataset with synthetic speech generated using publicly available implementations of diffusion-based models and hybrid models. Together, these systems span four major categories of generative speech technologies:

- 1) GAN-based models: These models learn to generate waveforms using adversarial training. We include MelGAN Large (MG-L) [48], Parallel WaveGAN (PWG) [49], Multi-band MelGAN (MB-MG) [50], HiFi-GAN (HF-G) [51], Avocodo (Avo) [52], and BigVGAN (BVG) [53].
- 2) Flow-based models: These systems use invertible transformations to generate waveform distributions. We include WaveGlow (WGlow) [35].
- 3) Diffusion-based models: These generate speech through iterative denoising of noise samples. We include FastDiff and ProDiff [36], [54], using their official pretrained models.<sup>3</sup>
- 4) Hybrid-based models: These combine signal processing techniques with neural networks. We include the Neural Source-Filter (NSF) model [37].<sup>4</sup>

This collection forms a reproducible benchmark covering all major generative paradigms in modern speech synthesis.

**JSUT Benchmark (Japanese).** To evaluate cross-lingual generalization, we use the JSUT corpus [55], a single-speaker Japanese dataset. Specifically, we use the basic5000 subcorpus, which contains 5,000 utterances. For synthetic counterparts, we utilize audio samples generated by PWG and MB-MelGAN models from the WaveFake dataset [16], which are based on the basic5000. This setup allows us to assess the robustness of attribution methods under language and domain shifts.

**ASVspoof LA Benchmark (VCTK-based, English).** To evaluate attribution performance in a multi-speaker, open-world setting, we use the ASVspoof 2019 Logical Access (LA) corpus [56], which is derived from the Voice Cloning Toolkit (VCTK) dataset [57]. VCTK contains recordings from 107 English speakers (46 male, 61 female) and is partitioned into disjoint training, development, and evaluation speaker sets. The ASVspoof LA corpus includes both genuine human speech (labeled as *bonafide*) and synthetically generated audio from a range of systems (labeled from A01 to A19). The training set consists of 2,580 genuine utterances and 22,800 synthetic utterances produced using four TTS and two VC systems. The development set follows a similar distribution, using the same synthetic systems as the training set. The evaluation set comprises 7,355 genuine utterances and 63,882 synthetic utterances generated using 13 different systems—of which 6 TTS and 5 VC systems are not present in the training set, while 1 TTS and 1 VC system are shared with it. In total, the dataset spans 17 different synthesis systems, making it a comprehensive benchmark

for synthetic speech detection and model attribution in realistic, multi-speaker scenarios.

## 5.2. Single-Model Attribution in an Open-World Setting

**Experimental Setup.** To determine whether an audio sample originates from a specific target synthesis system, we define a binary attribution task using residual vectors  $\mathcal{R}_{\text{test}}$  compared with a known fingerprint  $\hat{\mathcal{F}}$ . We evaluate two attribution scoring functions—correlation-based and Mahalanobis distance-based—across multiple residual feature types, including EnCodec and spectral filtering (low-pass, high-pass, band-stop, and band-pass). All residual features are derived from STFT-based acoustic representations.

For each feature type, we report the performance using its best-performing scoring function, selected based on the validation Area Under the Receiver Operating Characteristic Curve (AUROC). This allows a fair comparison between the EnCodec and the spectral filtering-based approach, each using its optimal configuration. The full set of evaluated configurations and their results—used to determine the best-performing settings reported here—is provided in Appendix A. The selected best-performing configurations include:

- EnCodec: Compression at 24 kbps, using the correlation-based score and an STFT window size of 2,048, and hop size of 128.
- Low-pass filter: Cutoff frequency at 1 kHz, with a stopband frequency at 1.5 kHz, using the Mahalanobis distance-based attribution score, and an STFT window size of 128, and a hop size of 2.

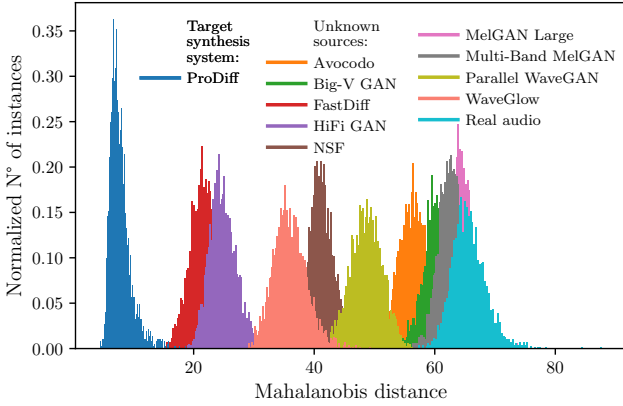
For each target synthesis system, a fingerprint is computed using 80% of its available samples. The remaining 20% are used for testing on a balanced set composed of 50% samples from the target system and 50% from non-target sources (i.e., other synthesis systems or real speech).

For the ASVspoof 2019 LA dataset, which is inherently imbalanced, we first combine the training and development sets (containing only categories A01–A06), and then split each into 80% training and 20% testing. To evaluate performance under open-world conditions with unseen synthesis types, we supplement the test set with data from the evaluation partition (A07–A19), sampling an equal number of test samples per category to match the amount taken from A01–A06 test splits. This yields a balanced test set that includes both known and unseen sources. We report the AUROC to quantify attribution performance without requiring a fixed decision threshold. As an example, Figure 3 shows the  $s_{\text{md}}$  between a target system’s fingerprint and various unseen inputs, including real audio, samples from other synthesis systems, and samples from the target system itself.

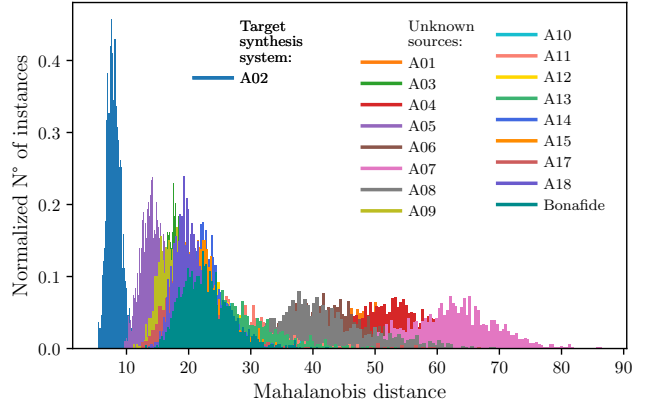
**Results.** The goal is to assess how well the fingerprint enables discrimination between the target system’s outputs and those from all other sources. Tables 1, 2, and 3 present

3. <https://github.com/Rongjiehuang/ProDiff>.

4. <https://github.com/nii-yamagishilab/project-NN-Pytorch-scripts?tab=readme-ov-file>.



(a) ProDiff model attribution assessment by scoring unseen inputs from various sources, including samples generated by the ProDiff model itself, using the Augmented LJSpeech Benchmark.



(b) A02 model attribution assessment by scoring unseen inputs from various sources, including samples generated by the A02 model itself, using the ASVspoof LA Benchmark.

Figure 3: Mahalanobis distance-based attribution results for two target synthesis systems: (a) ProDiff and (b) A02. In both cases, lower distances indicate that a sample is more likely to stem from the corresponding target system.

TABLE 1: AUROC scores for single-model attribution in an open-world setting using the English Augmented LJSpeech Benchmark. Each row represents a source: either real audio, samples from various synthesis systems, or samples from the target system itself. Each column corresponds to a target synthesis system. Values show the average AUROC over five runs using low-pass filtering and EnCodec-based residuals (reported as Low-pass / EnCodec). Higher scores indicate better discrimination between the target system and the others.

Source \ Target	FastDiff	ProDiff	MG-L	Avo	BVG	HF-G	MB-MG	PWG	WGlow	NSF
FastDiff	-	1.00 / 1.00	1.00 / 1.00	1.00 / 1.00	1.00 / 1.00	1.00 / 1.00	1.00 / 1.00	1.00 / 1.00	1.00 / 1.00	1.00 / 1.00
ProDiff	1.00 / 0.98	-	1.00 / 1.00	1.00 / 1.00	1.00 / 1.00	1.00 / 1.00	1.00 / 1.00	1.00 / 1.00	1.00 / 1.00	1.00 / 1.00
MG-L	1.00 / 0.98	1.00 / 1.00	-	1.00 / 1.00	1.00 / 1.00	1.00 / 1.00	1.00 / 1.00	1.00 / 1.00	1.00 / 1.00	1.00 / 1.00
Avo	1.00 / 1.00	1.00 / 1.00	1.00 / 1.00	-	1.00 / 0.99	1.00 / 1.00	1.00 / 0.96	0.99 / 0.97	1.00 / 0.99	1.00 / 0.80
BVG	1.00 / 1.00	1.00 / 1.00	1.00 / 1.00	1.00 / 0.97	-	1.00 / 1.00	1.00 / 0.98	0.99 / 0.98	1.00 / 0.98	1.00 / 0.94
HF-G	1.00 / 1.00	1.00 / 1.00	1.00 / 1.00	1.00 / 1.00	1.00 / 1.00	-	1.00 / 1.00	1.00 / 1.00	1.00 / 0.99	1.00 / 0.94
MB-MG	1.00 / 1.00	1.00 / 1.00	1.00 / 1.00	1.00 / 0.91	1.00 / 0.98	1.00 / 1.00	-	0.99 / 0.96	1.00 / 0.99	1.00 / 0.93
PWG	1.00 / 1.00	1.00 / 1.00	1.00 / 1.00	0.99 / 0.98	0.99 / 1.00	1.00 / 0.99	0.99 / 0.99	-	1.00 / 0.98	0.99 / 0.80
WGlow	1.00 / 1.00	1.00 / 1.00	1.00 / 1.00	1.00 / 1.00	1.00 / 1.00	1.00 / 0.98	1.00 / 1.00	1.00 / 0.99	-	1.00 / 0.92
NSF	1.00 / 1.00	1.00 / 1.00	1.00 / 1.00	1.00 / 0.99	1.00 / 1.00	1.00 / 0.98	1.00 / 1.00	1.00 / 0.98	1.00 / 0.99	-
Real	1.00 / 1.00	1.00 / 1.00	1.00 / 1.00	1.00 / 0.97	1.00 / 0.99	1.00 / 1.00	1.00 / 0.95	1.00 / 0.99	1.00 / 1.00	1.00 / 0.96
Avg.	1.00 / 1.00	1.00 / 1.00	1.00 / 1.00	1.00 / 0.98	1.00 / 1.00	1.00 / 1.00	1.00 / 0.99	1.00 / 0.99	1.00 / 0.99	1.00 / 0.93

the average AUROC scores for pairwise single-model attribution using synthetically generated speech based on the Augmented LJSpeech Benchmark, the ASVspoof LA Benchmark, and the JSUT Benchmark respectively.

For the Augmented LJSpeech Benchmark (Table 1), the AUROC reaches 1.0 in most cases—including comparisons among diffusion, GAN, flow, and hybrid-based models—indicating perfect separation. Some exceptions occur with EnCodec-based residuals. For example, when distinguishing NSF-generated samples from those of Avo or PWG, the AUROC drops to 0.80. However, applying our low-pass filtering strategy boosts performance in those cases to 1.0 and 0.99, respectively. We attribute this improvement to the reduced intra-class variance and increased inter-class fingerprint separability achieved by the low-pass filtering method.

For the ASVspoof LA Benchmark, the results in Table 2 show that low-pass residual features yield excellent attribution performance, with AUROC scores of 1.00 in most

cases. However, a few combinations where the source and target systems share architectural similarities result in lower scores. For instance, the A03-targeted fingerprint performs poorly in distinguishing A02 samples (AUROC = 0.78). This can be attributed to the architectural similarity between the two systems: both are neural TTS models that use the same waveform generator and rely on similar acoustic features such as F0, Mel-cepstral coefficients (MCCs), and band aperiodicity coefficients. These shared characteristics likely result in overlapping high-frequency residuals, making differentiation more challenging. Interestingly, the reverse comparison—A02 distinguishing A03—yields a perfect AUROC of 1.00, suggesting that the fingerprint derived from A02 captures more distinctive residual traits. In contrast, the fingerprint tailored to A03 may generalize less effectively, potentially due to higher intra-class variability or less discriminative spectral patterns. Another case is A01 vs. A04, which shows an AUROC of 0.87. Although the waveform generators differ, the use of interpolated F0 and MCCs

TABLE 2: AUROC scores for single-model attribution in an open-world setting using the English ASVspoof LA Benchmark. Each row represents a source: either real audio, samples from various synthesis systems, or samples from the target system itself. Each column corresponds to a target synthesis system. Values show the average AUROC over five runs using low-pass filtering and EnCodec-based residuals (reported as Low-pass / EnCodec). Higher scores indicate better discrimination between the target system and the others. VC systems are indicated with <sup>\*</sup>, and systems combining both TTS and VC are marked with <sup>‡</sup>. Systems without annotations correspond to TTS-only models. Systems A16 and A19 are excluded as they use the same synthesis pipelines as A04 and A06, respectively.

Src\Tgt	A01	A02	A03	A04	A05*	A06*
A01	-	1.00 / 1.00	1.00 / 1.00	0.87 / 0.82	1.00 / 1.00	1.00 / 0.97
A02	1.00 / 1.00	-	0.78 / 0.86	1.00 / 1.00	0.93 / 0.66	1.00 / 1.00
A03	1.00 / 1.00	1.00 / 0.97	-	1.00 / 1.00	1.00 / 0.99	1.00 / 1.00
A04	0.97 / 0.62	1.00 / 1.00	1.00 / 1.00	-	1.00 / 1.00	1.00 / 0.84
A05*	1.00 / 1.00	1.00 / 0.72	0.95 / 0.89	1.00 / 1.00	-	1.00 / 1.00
A06*	0.97 / 0.88	1.00 / 1.00	1.00 / 1.00	0.77 / 0.80	1.00 / 1.00	-
A07	0.99 / 0.54	1.00 / 1.00	1.00 / 1.00	0.95 / 0.62	1.00 / 1.00	1.00 / 0.92
A08	1.00 / 0.97	1.00 / 1.00	1.00 / 1.00	1.00 / 0.97	1.00 / 1.00	1.00 / 0.94
A09	1.00 / 1.00	1.00 / 0.99	0.94 / 0.84	1.00 / 1.00	0.99 / 0.99	1.00 / 1.00
A10	1.00 / 1.00	1.00 / 0.99	0.98 / 0.94	1.00 / 1.00	1.00 / 0.99	1.00 / 1.00
A11	1.00 / 1.00	1.00 / 0.99	1.00 / 0.93	1.00 / 1.00	1.00 / 0.99	1.00 / 1.00
A12	1.00 / 1.00	1.00 / 0.99	1.00 / 0.94	1.00 / 1.00	1.00 / 0.99	1.00 / 1.00
A13 <sup>‡</sup>	1.00 / 1.00	1.00 / 1.00	1.00 / 0.96	1.00 / 1.00	1.00 / 1.00	1.00 / 1.00
A14 <sup>‡</sup>	1.00 / 1.00	1.00 / 0.99	1.00 / 0.95	1.00 / 1.00	1.00 / 0.99	1.00 / 1.00
A15 <sup>‡</sup>	1.00 / 1.00	1.00 / 0.95	0.98 / 0.82	1.00 / 1.00	1.00 / 0.95	1.00 / 1.00
A17*	1.00 / 1.00	1.00 / 0.90	0.97 / 0.90	1.00 / 1.00	0.99 / 0.79	1.00 / 0.99
A18*	1.00 / 1.00	1.00 / 0.98	0.99 / 0.97	0.99 / 1.00	1.00 / 0.97	1.00 / 0.97
BonaFide	1.00 / 0.94	1.00 / 0.92	0.99 / 0.92	1.00 / 0.95	1.00 / 0.89	1.00 / 0.99
Avg.	1.00 / 0.94	1.00 / 0.96	0.97 / 0.94	0.97 / 0.95	0.99 / 0.95	1.00 / 0.98

TABLE 3: AUROC scores for single-model attribution using the Japanese JSUT Benchmark. Each row indicates a source (e.g., synthesis system or real audio), and columns represent target synthesis systems. Values show the average AUROC over five runs using low-pass and EnCodec-based fingerprinting (reported as Low-pass / EnCodec). Higher values indicate better attribution performance.

Source \ Target	PWG	MB-MG
PWG	-	1.00 / 0.99
MB-MG	1.00 / 1.00	-
Real	1.00 / 1.00	1.00 / 1.00
Avg.	1.00 / 1.00	1.00 / 1.00

in A01 resembles the prosodic features used for join-cost computation in A04, reducing discriminability. The A06 vs. A04 pair, with an AUROC of 0.77, also illustrates this trend. A06 is a VC system that uses transfer-function filtering of residuals, whereas A04 is a TTS system based on waveform concatenation; both methods aim to preserve natural waveform characteristics, which may result in less distinguishable low-pass residuals. EnCodec residuals also achieve high AUROC values overall but exhibit greater variability, particularly for the more similar system pairs mentioned above. This could be attributed to the lossy nature of EnCodec’s compression and neural reconstruction, which may mask fine-grained artifacts. In contrast, low-pass residuals retain and enhance subtle inconsistencies in the high-frequency spectrum, making them more sensitive to system-specific

characteristics when present. The average AUROC scores reflect these patterns: low-pass residuals consistently yield averages between 0.97 and 1.00, while EnCodec residuals range from 0.94 to 0.98, indicating slightly lower and more variable attribution performance. A detailed description of each synthesis system (A01–A19) can be found in the official ASVspoof 2019 LA documentation [56].

Table 3 presents AUROC results for single-model attribution using the Japanese JSUT Benchmark. The results show that the PWG and MB-MG synthesis systems achieve near-perfect AUROC scores across all pairwise comparisons, demonstrating effective attribution performance in an additional language.

Overall, these results demonstrate that our fingerprinting approach enables robust, fine-grained attribution of synthetic speech to its source system with near-perfect accuracy, even in challenging open-world conditions involving diverse and highly similar generation models. Notably, the method not only excels at distinguishing among synthetic systems but also consistently separates real from synthetic speech — underscoring its robustness across languages and generation paradigms. This level of attribution fidelity highlights the potential of residual-based fingerprints as a powerful tool for audio provenance analysis in real-world scenarios, such as misinformation detection and synthetic media forensics.

**Noise Robustness.** In addition to testing attribution performance, we evaluate the resilience of our Augmented LJSpeech Benchmark fingerprints to additive environmental noise using samples from the MUSAN corpus [58], which includes 843 recordings of music, speech, and background sounds. Noise is added at varying signal-to-noise ratios (SNRs) from 0 dB to 40 dB using the SpeechBrain augmentation toolkit, where higher SNR values indicate less noise and cleaner signals.<sup>5</sup> Figure 4 illustrates the noise robustness of our fingerprinting approach. We observe average AUROC scores above 0.80 for SNRs greater than 15 dB, indicating strong attribution performance under moderate to low noise conditions. While these results are promising, we recognize that in critical large-scale detection scenarios—where even a 1% false positive rate may be considered high—an AUROC of 0.80 might not yet be sufficient. Notably, no dataset augmentation was applied during training to improve noise resilience, which remains a promising direction for future work.

### 5.3. Multi-Model Attribution in a Closed-World Setting

**Experimental Setup.** We evaluate closed-world attribution on the Augmented LJSpeech Benchmark, using 80% training, 10% validation, and 10% testing across 10 synthesis systems. We compare our fingerprint approach against state-of-the-art baseline models.

5. <https://speechbrain.readthedocs.io/en/v0.5.9/API/speechbrain.lobes.augment.html>.

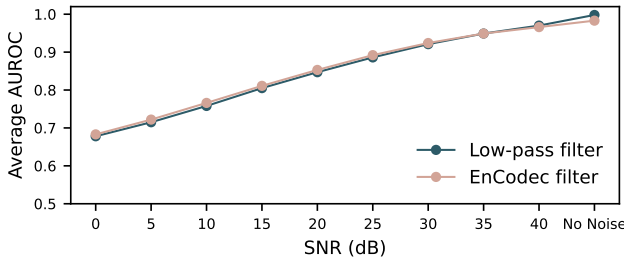


Figure 4: Average AUROC for single-model attribution across varying noise levels measured in SNR (dB) using the English Augmented LJSpeech Benchmark.

**Fingerprint:** For our proposed method, we use our pre-computed fingerprints for each synthesis system, as described in Section 5.2, relying on the low-pass filter residual feature extraction method, which yielded the best performance (see Table 1). We aim to classify each test sample as originating from one of  $m = 10$  known synthesis systems. Each system is associated with a precomputed fingerprint  $\hat{\mathcal{F}}_m$ , which summarizes its characteristic residual energy pattern. To predict the source system of a given test sample, we compute the Mahalanobis distance between the test residual  $\mathcal{R}_{\text{test}}$  and each fingerprint. The synthesis system with the smallest distance is selected as the predicted label  $\hat{y}_{\text{md}}$ :

$$\hat{y}_{\text{md}} = \arg \min_{m \in \{1, \dots, 10\}} d_{\text{md}}(\mathcal{R}_{\text{test}}, \hat{\mathcal{F}}_m).$$

**Baseline methods:** We compare our method against five baseline models, each adapted to our multi-model attribution setting: X-vector [59], LCNN [60], ResNet [61], SE-ResNet [62], and VFD-Net [13]. All models are trained for 100 epochs with the Adam optimizer (learning rate 0.001,  $\beta = (0.9, 0.98)$ ) using a linear learning rate scheduler and a warm-up phase of 100 iterations. Cross-entropy loss is used for classification unless otherwise specified. Class probabilities are obtained via softmax, and predictions are generated by taking the argmax over these probabilities. Detailed architecture descriptions and preprocessing setups for each baseline are provided in Appendix B. All baseline models operate in a closed-world setting and thus are not suitable for open-world detection.

We report accuracy, F1-score, precision, and recall averaged over five independent trials. All metrics are computed per class and then averaged using macro-averaging, treating all classes equally. We ensure a balanced evaluation by using an equal number of samples per class.

**Results.** Table 4 shows that our fingerprinting method significantly outperforms all baselines across accuracy, F1-score, precision, and recall. The statistical significance of the improvement is confirmed by a Wilcoxon Rank-Sum Test with a p-value of 0.009, below the standard threshold of  $\alpha = 0.05$ .

TABLE 4: Multi-model attribution in a closed-world setting results comparing our fingerprinting approach to state-of-the-art methods, using the English Augmented LJSpeech Benchmark. Results are averaged over five trials, with standard deviations shown in parentheses.

Methods	Accuracy	F1-score	Precision	Recall
X-vector	0.999 (0.000)	0.999 (0.000)	0.999 (0.000)	0.999 (0.000)
LCNN	0.968 (0.023)	0.968 (0.022)	0.974 (0.014)	0.968 (0.023)
ResNet	0.997 (0.000)	0.997 (0.000)	0.997 (0.000)	0.997 (0.000)
SE-ResNet	0.997 (0.001)	0.997 (0.001)	0.997 (0.001)	0.997 (0.001)
VFD-Net	0.968 (0.004)	0.968 (0.004)	0.968 (0.004)	0.968 (0.004)
<b>Fingerprint</b>	<b>1.000 (0.000)</b>	<b>1.000 (0.000)</b>	<b>1.000 (0.000)</b>	<b>1.000 (0.000)</b>

#### 5.4. Real vs. Synthetic Detection

**Experimental Setup.** This binary classification task uses the same Augmented LJSpeech Benchmark split, reusing the closed-world data split. To ensure class balance, we oversample real speech samples to match the number of synthetic ones. We evaluate two fingerprint-based methods and compare their performance against baseline models for detecting real vs. synthetic speech:

**1) Neural Network-Based Fingerprinting.** This method uses low-pass residual features (Equation 1) fed into a three-layer neural network (128–64–32 units), trained with batch norm, dropout (0.5), and ReLU activations. The final layer outputs a single scalar logit, which is passed through a sigmoid activation to indicate the probability that the input is synthetically generated. The network is initialized using Kaiming normal initialization and trained with the Adam optimizer (learning rate 0.001), together with a linear learning rate scheduler featuring 100 warm-up iterations.

**2) Training-Free Fingerprinting.** In contrast, we also explore a training-free alternative that does not involve learning a classifier. For each test sample, we compute its residual  $\mathcal{R}_{\text{test}}$  and calculate the Mahalanobis distance to all available fingerprints, selecting the minimum distance value. This minimum is compared to a threshold  $\tau$ : if the distance is below  $\tau$ , the sample is classified as synthetic; otherwise, it is labeled as real. The threshold  $\tau$  is determined using a 10% held-out validation set. We sweep a range of candidate thresholds and select the one that maximizes the F1 score on the validation data. This selected  $\tau$  is then applied to the test set using the same decision rule. This method relies on the intuition that synthetic samples are more likely to produce residuals closely matching a known fingerprint, leading to smaller Mahalanobis distances.

Baseline models, described in Section 5.3, are re-trained and adapted to use binary cross-entropy loss. Logits are passed through a sigmoid function, and predictions are thresholded at 0.5, assigning each sample to class 0 (real) or 1 (synthetic). We report accuracy, F1-score, precision, and recall averaged over five independent trials.

**Results.** Table 5 presents the performance comparison between our fingerprinting approaches and state-of-the-

TABLE 5: Performance comparison of our fingerprinting approaches against state-of-the-art methods for detecting synthetic speech versus real audio, using the English Augmented LJSpeech Benchmark. Results are averaged over five trials, with standard deviations shown in parentheses.

Methods	Accuracy	F1	Precision	Recall
X-vector	0.977 (0.010)	0.978 (0.010)	0.958 (0.020)	<b>0.999 (0.001)</b>
LCNN	0.985 (0.008)	0.985 (0.008)	0.979 (0.016)	0.991 (0.004)
ResNet	0.992 (0.001)	0.992 (0.001)	0.990 (0.003)	0.994 (0.002)
SE-ResNet	0.992 (0.002)	0.992 (0.002)	0.989 (0.004)	0.994 (0.003)
VFD-Net	0.985 (0.002)	0.985 (0.002)	0.985 (0.003)	0.986 (0.002)
Fingerprint (Free)	0.974 (0.002)	0.973 (0.002)	0.987 (0.005)	0.960 (0.003)
<b>Fingerprint (NN)</b>	<b>0.997 (0.001)</b>	<b>0.997 (0.001)</b>	<b>0.996 (0.001)</b>	0.998 (0.000)

art baselines for detecting synthetic speech. Our neural-network-based fingerprint model, labeled Fingerprint (NN), outperforms all baselines in accuracy, F1, and precision, demonstrating the strong capability of learned residual representations for synthetic speech detection. Statistical significance tests using the Wilcoxon Rank-Sum Test confirm that these improvements over all baselines are significant ( $p < 0.05$ ). While our method also leads in recall, its advantage over the X-vector is less pronounced ( $p = 0.117$ ).

In addition, we evaluate a training-free version, labeled Fingerprint (Free). Despite its simplicity, this approach performs competitively—achieving an F1 score of 0.973 and surpassing several deep learning baselines in precision. This result highlights the robustness of the residual fingerprint representation itself. Moreover, we expect the performance of the training-free approach to improve further as the number and diversity of available fingerprints increase, potentially enhancing its generalization and detection capability.

Together, these results highlight the inherent strength of the residual fingerprints themselves, and demonstrate the strong effectiveness of our approach for reliable synthetic speech detection.

## 6. Discussion and Conclusion

With speech generation models achieving remarkable realism and ease of use—or misuse—the need for effective spoofing detection and synthesis system attribution in both open- and closed-world settings is growing rapidly, making them critical components for securing voice-based communication systems, mitigating misinformation, and ensuring the integrity of biometric authentication. Our proposed fingerprinting approach—using either EnCodec or low-pass filtered residuals—demonstrates strong performance across a wide range of evaluation settings. Unlike most existing classification-based methods for audio deepfake detection, our approach is simple to implement and leverages lightweight signal-level artifacts rather than complex model training, offering a practical and scalable alternative to the model attribution and deepfake detection toolbox.

### Single-Model Attribution in an Open-World Setting:

Our method achieves near-perfect AUROC scores when distinguishing samples generated by a target synthesis system from unknown systems and real audio, demonstrating strong robustness and generalization without extensive training.

**Multi-Model Attribution in a Closed-World Setting:** Using residual fingerprints, our approach outperforms deep-learning baselines while remaining lightweight and interpretable, reliably identifying the correct synthesis source among known candidates.

**Real vs. Synthetic Detection:** Even in a training-free setup, our method effectively separates synthetic from real audio, highlighting the strength of residual fingerprints as a signal-level detection cue—particularly useful in low-resource or rapid-response scenarios. With minimal effort, performance can be further improved by training a simple neural network, achieving results that surpass current state-of-the-art methods.

**Robustness:** We further demonstrate that our single-model attribution framework proves effective in noise conditions, maintaining good performance ( $\text{SNR} \geq 15 \text{ dB}$ ), which further underscores its practicality.

**Research implications:** This work contributes to the growing field of audio deepfake forensics by emphasizing single-model open-world attribution, a realistic and highly challenging setting that remains underexplored. Unlike multi-class classification, where all possible synthesis systems are assumed known, open-world attribution more closely mirrors real-world scenarios—especially in adversarial settings where attackers can train and deploy proprietary models. Research in this direction can advance more generalizable and scalable forensic tools.

**Limitations:** Our single-model attribution setting relies on some access to target samples to construct a reliable fingerprint. In scenarios where an attacker uses a privately trained or unreleased model, collecting such data may be challenging.

**Extensions:** While we focus on low-pass and EnCodec-based residuals, our modular framework supports other signal decompositions. Appendix A shows that mid-frequency filters are also effective, suggesting room for task-specific tuning. Future work could examine the role of fingerprint robustness under transformations such as bandwidth variation, bit rate changes, or neural re-synthesis. Understanding how different synthesis systems leave distinct fingerprints may unlock further opportunities for model attribution, tampering detection, and content provenance.

## References

[1] B. Yan, J. Shi, Y. Tang, H. Inaguma, Y. Peng, S. Dalmia, P. Polák, P. Fernandes, D. Berrebbi, T. Hayashi, X. Zhang, Z. Ni, M. Hira, S. Maiti, J. Pino, and S. Watanabe, “ESPnet-ST-v2: Multipurpose spoken language translation toolkit,” in *Proceedings of the 61st Annual Meeting of the Association for Computational Linguistics (Volume 3: System Demonstrations)*. Association for Computational Linguistics, 2023, pp. 400–411.

[2] M. Ravanelli, T. Parcollet, A. Moumen, S. de Langen, C. Subakan, P. Plantinga, Y. Wang, P. Mousavi, L. D. Libera, A. Ploujnikov, F. Paissan, D. Borra, S. Zaiem, Z. Zhao, S. Zhang, G. Karakasidis, S.-L. Yeh, P. Champion, A. Rouhe, R. Braun, F. Mai, J. Zuluaga-Gomez, S. M. Mousavi, A. Nautsch, X. Liu, S. Sagar, J. Duret, S. Mdhaffar, G. Laperriere, M. Rouvier, R. D. Mori, and Y. Esteve, “Open-source conversational AI with speechbrain 1.0,” 2024.

[3] S. L. Metzger, K. T. Littlejohn, A. B. Silva, D. A. Moses, M. P. Seaton, R. Wang, M. E. Dougherty, J. R. Liu, P. Wu, M. A. Berger, I. Zhuravleva, A. Tu-Chan, K. Ganguly, G. K. Anumanchipalli, and E. F. Chang, “A high-performance neuroprosthesis for speech decoding and avatar control,” *Nature*, vol. 620, pp. 1037–1046, 2023.

[4] R. Badlani, R. Valle, K. J. Shih, J. F. Santos, S. Gururani, and B. Catanzaro, “RAD-MMM: Multilingual Multiaccented Multispeaker Text To Speech,” in *Proc. Interspeech*, 2023, pp. 626–630.

[5] N. Bontridder and Y. Poulet, “The role of artificial intelligence in disinformation,” *Data N°38: Policy*, vol. 3, p. e32, 2021.

[6] P. Gupta, H. A. Patil, and R. C. Guido, “Vulnerability issues in automatic speaker verification (ASV) systems,” *EURASIP Journal on Audio, Speech, and Music Processing*, vol. 10, 2024.

[7] R. A. Delfino, “Deepfakes on trial: A call to expand the trial judge’s gatekeeping role to protect legal proceedings from technological fakery,” *Hastings Law Journal*, vol. 74, no. 2, p. 293, 2023.

[8] D. Dai, Y. Chen, L. Chen, M. Tu, L. Liu, R. Xia, Q. Tian, Y. Wang, and Y. Wang, “Cloning one’s voice using very limited data in the wild,” in *ICASSP 2022 - 2022 IEEE International Conference on Acoustics, Speech and Signal Processing (ICASSP)*, 2022, pp. 8322–8326.

[9] K. Klapsas, N. Ellinas, K. Nikitaras, G. Vamvoukakis, P. Kakoulidis, K. Markopoulos, S. Raptis, J. S. Sung, G. Jho, A. Chalamandaris, and P. Tsiaikoulis, “Self supervised learning for robust voice cloning,” in *Proc. Interspeech*, 2022, pp. 4935–4939.

[10] X. Wang, H. Delgado, H. Tak, J.-w. Jung, H.-j. Shim, M. Todisco, I. Kukanov, X. Liu, M. Sahidullah, T. Kinnunen, N. Evans, K. A. Lee, and J. Yamagishi, “ASVspoof 5: Crowdsourced speech data, deepfakes, and adversarial attacks at scale,” in *ASVspoof Workshop*, 2024.

[11] J. Yi, J. Tao, R. Fu, X. Yan, C. Wang, T. Wang, C. Y. Zhang, X. Zhang, Y. Zhao, Y. Ren, L. Xu, J. Zhou, H. Gu, Z. Wen, S. Liang, Z. Lian, S. Nie, and H. Li, “ADD 2023: the second audio deepfake detection challenge,” in *DADA@IJCAI*, 2023.

[12] X. Yan, J. Yi, J. Tao, C. Wang, H. Ma, T. Wang, S. Wang, and R. Fu, “An initial investigation for detecting vocoder fingerprints of fake audio,” in *Proceedings of the 1st International Workshop on Deepfake Detection for Audio Multimedia*, ser. DDAM ’22. New York, NY, USA: Association for Computing Machinery, 2022, p. 61–68.

[13] J. Deng, Y. Ren, T. Zhang, H. Zhu, and Z. Sun, “VFD-Net: Vocoder Fingerprints Detection for Fake Audio,” in *ICASSP*, 2024, pp. 12 151–12 155.

[14] Y. Wang, R. Skerry-Ryan, D. Stanton, Y. Wu, R. J. Weiss, N. Jaitly, Z. Yang, Y. Xiao, Z. Chen, S. Bengio, Q. Le, Y. Agiomyrgiannakis, R. Clark, and R. A. Saurous, “Tacotron: Towards End-to-End Speech Synthesis,” in *Proc. Interspeech 2017*, 2017, pp. 4006–4010.

[15] T. Kaneko, H. Kameoka, K. Hiramatsu, and K. Kashino, “Sequence-to-Sequence Voice Conversion with Similarity Metric Learned Using Generative Adversarial Networks,” in *Interspeech 2017*, 2017, pp. 1283–1287.

[16] J. Frank and L. Schönherr, “WaveFake: A Data Set to Facilitate Audio Deepfake Detection,” in *Thirty-fifth Conference on Neural Information Processing Systems Datasets and Benchmarks Track*, 2021.

[17] F. Li, Y. Chen, H. Liu, Z. Zhao, Y. Yao, and X. Liao, “Vocoder Detection of Spoofing Speech Based on GAN Fingerprints and Domain Generalization,” *ACM Trans. Multimedia Comput. Commun. Appl.*, vol. 20, no. 6, mar 2024.

[18] X. Zhou, D. Garcia-Romero, R. Duraiswami, C. Espy-Wilson, and S. Shamma, “Linear versus mel frequency cepstral coefficients for speaker recognition,” in *2011 IEEE Workshop on Automatic Speech Recognition & Understanding*, 2011, pp. 559–564.

[19] M. Todisco, H. Delgado, and N. Evans, “Constant Q cepstral coefficients: A spoofing countermeasure for automatic speaker verification,” *Computer Speech & Language*, vol. 45, pp. 516–535, 2017.

[20] J. Li, H. Wang, P. He, S. M. Abdullahi, and B. Li, “Long-term variable Q transform: A novel time-frequency transform algorithm for synthetic speech detection,” *Digital Signal Processing*, vol. 120, p. 103256, 2022.

[21] Z. Ji, Z.-Y. Li, P. Li, M. An, S. Gao, D. Wu, and F. Zhao, “Ensemble Learning for Countermeasure of Audio Replay Spoofing Attack in ASVspoof2017,” in *Proc. Interspeech*, 2017, pp. 87–91.

[22] D. Snyder, D. Garcia-Romero, A. McCree, G. Sell, D. Povey, and S. Khudanpur, “Spoken Language Recognition using X-vectors,” in *The Speaker and Language Recognition Workshop*, 2018.

[23] Z. Wu, R. K. Das, J. Yang, and H. Li, “Light Convolutional Neural Network with Feature Genuinization for Detection of Synthetic Speech Attacks,” in *Proc. Interspeech*, 2020, pp. 1101–1105.

[24] A. Chinthia, B. Thai, S. J. Sohrawardi, K. Bhatt, A. Hickerson, M. Wright, and R. Ptucha, “Recurrent convolutional structures for audio spoof and video deepfake detection,” *IEEE Journal of Selected Topics in Signal Processing*, vol. 14, no. 5, pp. 1024–1037, 2020.

[25] M. Alzantot, Z. Wang, and M. B. Srivastava, “Deep Residual Neural Networks for Audio Spoofing Detection,” in *Proc. Interspeech*, 2019, pp. 1078–1082.

[26] Y. Yang, H. Wang, H. Dinkel, Z. Chen, S. Wang, Y. Qian, and K. Yu, “The SJTU Robust Anti-Spoofing System for the ASVspoof 2019 Challenge,” in *Proc. Interspeech 2019*, 2019, pp. 1038–1042.

[27] J. Kim and S. M. Ban, “Phase-aware spoof speech detection based on Res2net with phase network,” in *ICASSP 2023 - 2023 IEEE International Conference on Acoustics, Speech and Signal Processing (ICASSP)*, 2023, pp. 1–5.

[28] C.-I. Lai, N. Chen, J. Villalba, and N. Dehak, “ASSERT: Anti-Spoofing with Squeeze-Excitation and Residual Networks,” in *Proc. Interspeech*, 2019, pp. 1013–1017.

[29] Y. Zhang, W. Wang, and P. Zhang, “The Effect of Silence and Dual-Band Fusion in Anti-Spoofing System,” in *Proc. Interspeech 2021*, 2021, pp. 4279–4283.

[30] H. Tak, J. Patino, M. Todisco, A. Nautsch, N. Evans, and A. Larcher, “End-to-End anti-spoofing with RawNet2,” in *ICASSP*, 2021, pp. 6369–6373.

[31] H. Tak, J. weon Jung, J. Patino, M. Todisco, and N. Evans, “Graph Attention Networks for Anti-Spoofing,” in *Proc. Interspeech*, 2021, pp. 2356–2360.

[32] J. Jung, H. Heo, H. Tak, H. Shim, J. Chung, B. Lee, H. Yu, and N. Evans, “AASIST: Audio anti-spoofing using integrated spectro-temporal graph attention networks,” in *2022 IEEE International Conference on Acoustics, Speech, and Signal Processing, ICASSP 2022 - Proceedings*, 2022, pp. 2405–2409.

[33] W. Ge, M. Panariello, J. Patino, M. Todisco, and N. Evans, “Partially-Connected Differentiable Architecture Search for Deepfake and Spoofing Detection,” in *Proc. Interspeech*, 2021, pp. 4319–4323.

[34] X. Liu, M. Liu, L. Wang, K. A. Lee, H. Zhang, and J. Dang, "Leveraging positional-related local-global dependency for synthetic speech detection," in *ICASSP*, 2023, pp. 1–5.

[35] R. Prenger, R. Valle, and B. Catanzaro, "Waveglow: A flow-based generative network for speech synthesis," in *ICASSP*, 2019, pp. 3617–3621.

[36] R. Huang, M. W. Lam, J. Wang, D. Su, D. Yu, Y. Ren, and Z. Zhao, "FastDiff: A Fast Conditional Diffusion Model for High-Quality Speech Synthesis," in *Proceedings of the Thirty-First International Joint Conferences on Artificial Intelligence*. IJCAI, 2022.

[37] X. Wang and J. Yamagishi, "Neural Harmonic-plus-Noise Waveform Model with Trainable Maximum Voice Frequency for Text-to-Speech Synthesis," in *10th ISCA Workshop on Speech Synthesis (SSW 10)*, 2019, pp. 1–6.

[38] J. Lu, Y. Zhang, Z. Li, Z. Shang, W. Wang, and P. Zhang, "Detecting unknown speech spoofing algorithms with nearest neighbors," in *DADA@IJCAI*, 2023.

[39] X. Qin, X. Wang, Y. Chen, Q. Meng, and M. Li, "From speaker verification to deepfake algorithm recognition: Our learned lessons from ADD2023 track 3," in *DADA@IJCAI*, 2023.

[40] C.-y. Huang, Y. Y. Lin, H.-y. Lee, and L.-s. Lee, "Defending Your Voice: Adversarial Attack on Voice Conversion," in *2021 IEEE Spoken Language Technology Workshop (SLT)*, 2021, pp. 552–559.

[41] Z. Liu, Y. Zhang, and C. Miao, "Protecting Your Voice from Speech Synthesis Attacks," in *Proceedings of the 39th Annual Computer Security Applications Conference*, ser. ACSAC '23. New York, NY, USA: Association for Computing Machinery, 2023, p. 394–408.

[42] F. Marra, D. Gragnaniello, L. Verdoliva, and G. Poggi, "Do GANs leave artificial fingerprints?" in *2019 IEEE conference on multimedia information processing and retrieval (MIPR)*. IEEE, 2019, pp. 506–511.

[43] A. Défossez, J. Copet, G. Synnaeve, and Y. Adi, "High Fidelity Neural Audio Compression," *Transactions on Machine Learning Research*, 2023.

[44] A. Podolskiy, D. Lipin, A. Bout, E. Artemova, and I. Piontovskaya, "Revisiting mahalanobis distance for transformer-based out-of-domain detection," *Proceedings of the AAAI Conference on Artificial Intelligence*, vol. 35, no. 15, pp. 13 675–13 682, May 2021.

[45] F. Behrendt, D. Bhattacharya, R. Mieling, L. Maack, J. Krüger, R. Opfer, and A. Schlaefer, "Leveraging the mahalanobis distance to enhance unsupervised brain MRI anomaly detection," in *Medical Image Computing and Computer Assisted Intervention – MICCAI 2024: 27th International Conference, Marrakesh, Morocco, October 6–10, 2024, Proceedings, Part XI*. Berlin, Heidelberg: Springer-Verlag, 2024, p. 394–404.

[46] K. Ito and L. Johnson, "The LJ Speech Dataset," <https://keithito.com/LJ-Speech-Dataset/>, 2017.

[47] K. Gasenzer and M. Wolter, "Towards generalizing deep-audio fake detection networks," *Transactions on Machine Learning Research*, 2024.

[48] K. Kumar, R. Kumar, T. de Boissiere, L. Gestin, W. Z. Teoh, J. Sotelo, A. de Brébisson, Y. Bengio, and A. C. Courville, "Melgan: Generative adversarial networks for conditional waveform synthesis," in *Advances in Neural Information Processing Systems*, H. Wallach, H. Larochelle, A. Beygelzimer, F. d'Alché-Buc, E. Fox, and R. Garnett, Eds., vol. 32. Curran Associates, Inc., 2019.

[49] R. Yamamoto, E. Song, and J.-M. Kim, "Parallel wavegan: A fast waveform generation model based on generative adversarial networks with multi-resolution spectrogram," in *ICASSP 2020 - 2020 IEEE International Conference on Acoustics, Speech and Signal Processing (ICASSP)*, 2020, pp. 6199–6203.

[50] G. Yang, S. Yang, K. Liu, P. Fang, W. Chen, and L. Xie, "Multi-band melgan: Faster waveform generation for high-quality text-to-speech," in *Proceedings of the IEEE Spoken Language Technology Workshop (SLT)*, 2021.

[51] J. Kong, J. Kim, and J. Bae, "Hifi-gan: Generative adversarial networks for efficient and high fidelity speech synthesis," in *Advances in Neural Information Processing Systems*, H. Larochelle, M. Ranzato, R. Hadsell, M. Balcan, and H. Lin, Eds., vol. 33. Curran Associates, Inc., 2020, pp. 17 022–17 033.

[52] T. Bak, J. Lee, H. Bae, J. Yang, J.-S. Bae, and Y.-S. Joo, "Avocodo: generative adversarial network for artifact-free vocoder," in *Proceedings of the Thirty-Seventh AAAI Conference on Artificial Intelligence and Thirty-Fifth Conference on Innovative Applications of Artificial Intelligence and Thirteenth Symposium on Educational Advances in Artificial Intelligence*, ser. AAAI'23/IAAI'23/EAAI'23. AAAI Press, 2023.

[53] S. gil Lee, W. Ping, B. Ginsburg, B. Catanzaro, and S. Yoon, "BigVGAN: A universal neural vocoder with large-scale training," in *The Eleventh International Conference on Learning Representations*, 2023.

[54] R. Huang, Z. Zhao, H. Liu, J. Liu, C. Cui, and Y. Ren, "ProDiff: Progressive fast diffusion model for high-quality text-to-speech," in *Proceedings of the 30th ACM International Conference on Multimedia*, 2022.

[55] R. Sonobe, S. Takamichi, and H. Saruwatari, "JSUT corpus: free large-scale japanese speech corpus for end-to-end speech synthesis," *CoRR*, vol. abs/1711.00354, 2017.

[56] X. Wang, J. Yamagishi, M. Todisco, H. Delgado, A. Nautsch, N. Evans, M. Sahidullah, V. Vestman, T. Kinnunen, K. A. Lee, L. Juvela, P. Alku, Y.-H. Peng, H.-T. Hwang, Y. Tsao, H.-M. Wang, S. L. Maguer, M. Becker, F. Henderson, R. Clark, Y. Zhang, Q. Wang, Y. Jia, K. Onuma, K. Mushika, T. Kaneda, Y. Jiang, L.-J. Liu, Y.-C. Wu, W.-C. Huang, T. Toda, K. Tanaka, H. Kameoka, I. Steiner, D. Matrouf, J.-F. Bonastre, A. Govender, S. Ronanki, J.-X. Zhang, and Z.-H. Ling, "ASVspoof 2019: A large-scale public database of synthesized, converted and replayed speech," *Computer Speech & Language*, vol. 64, p. 10114, 2020.

[57] C. Veaux, J. Yamagishi, and K. MacDonald, "CSTR VCTK Corpus: English Multi-speaker Corpus for CSTR Voice Cloning Toolkit [sound]," 2017.

[58] T. Ko, V. Peddinti, D. Povey, M. L. Seltzer, and S. Khudanpur, "A study on data augmentation of reverberant speech for robust speech recognition," in *ICASSP*. IEEE, 2017, pp. 5220–5224.

[59] D. Snyder, D. Garcia-Romero, G. Sell, D. Povey, and S. Khudanpur, "X-Vectors: Robust DNN Embeddings for Speaker Recognition," in *2018 IEEE International Conference on Acoustics, Speech and Signal Processing (ICASSP)*, 2018, pp. 5329–5333.

[60] G. Lavrentyeva, S. Novoselov, A. Tseren, M. Volkova, A. Gorlanov, and A. Kozlov, "STC Antispoofing Systems for the ASVspoof2019 Challenge," in *Interspeech 2019*, 2019, pp. 1033–1037.

[61] K. He, X. Zhang, S. Ren, and J. Sun, "Deep residual learning for image recognition," in *2016 IEEE Conference on Computer Vision and Pattern Recognition (CVPR)*, 2016, pp. 770–778.

[62] J. Hu, L. Shen, and G. Sun, "Squeeze-and-excitation networks," in *2018 IEEE/CVF Conference on Computer Vision and Pattern Recognition*, 2018, pp. 7132–7141.

[63] A. Waibel, T. Hanazawa, G. Hinton, K. Shikano, and K. Lang, "Phoneme recognition using time-delay neural networks," *IEEE Transactions on Acoustics, Speech, and Signal Processing*, vol. 37, no. 3, pp. 328–339, 1989.

[64] V. Peddinti, D. Povey, and S. Khudanpur, "A time delay neural network architecture for efficient modeling of long temporal contexts," in *Interspeech 2015*, 2015, pp. 3214–3218.

[65] X. Wu, R. He, Z. Sun, and T. Tan, "A Light CNN for Deep Face Representation With Noisy Labels," *IEEE Transactions on Information Forensics and Security*, vol. 13, no. 11, pp. 2884–2896, 2018.

[66] P. Khosla, P. Teterwak, C. Wang, A. Sarna, Y. Tian, P. Isola, A. Maschinot, C. Liu, and D. Krishnan, "Supervised Contrastive Learning," in *Advances in Neural Information Processing Systems*, H. Larochelle, M. Ranzato, R. Hadsell, M. Balcan, and H. Lin, Eds., vol. 33. Curran Associates, Inc., 2020, pp. 18 661–18 673.

[67] R. Cipolla, Y. Gal, and A. Kendall, “Multi-task Learning Using Uncertainty to Weigh Losses for Scene Geometry and Semantics,” in *2018 IEEE/CVF Conference on Computer Vision and Pattern Recognition*, 2018, pp. 7482–7491.

## Appendix A. Evaluated Attribution Configurations

This appendix details the full range of evaluated configurations for the attribution task, including alternative residual feature representations and scoring methods. We report validation AUROC scores to compare different configurations and identify the best-performing settings used in the main results. We identify the optimal scoring function—either correlation or Mahalanobis distance—for each type of residual representation. Based on these evaluations, we report the best-performing configurations separately for EnCodec-based and spectral filtering-based residuals.

All evaluations are conducted using the ASVspoof 2019 Logical Access (LA) benchmark. Specifically, we train fingerprints for two synthesis systems—A16 and A19—which correspond to systems A04 and A06 in the training set. For these systems we use 95% of the available data for fingerprint construction, reserving the remaining 5% for testing. To ensure a fair and balanced evaluation, we also select an equivalent number of samples representing 5% of each system in the evaluation set (A07–A19). All of these data are used strictly for configuration selection.

### A.1. EnCodec

**Experimental Setup.** Residuals are extracted from audio compressed at 24 kbps and are evaluated in both correlation-based and Mahalanobis distance-based scoring using an STFT configuration with a window size of 128 and a hop size of 2.

**Results.** Based on Table 6, we select Pearson correlation as the attribution scoring metric, as it slightly outperforms Mahalanobis distance by achieving higher average AUROC on the validation set (0.97 vs. 0.96 for A16).

### A.2. Spectral Filtering

As with EnCodec, we compare correlation and Mahalanobis attribution scoring to identify the best-performing method for each spectral filter configuration using an STFT with a window size of 128 and a hop size of 2. Then we select the overall best-performing filter type.

**A.2.1. Low-pass filter setup.** This filter method retains only the low-frequency content below the cutoff, potentially emphasizing system-specific spectral characteristics in the lower bands. We evaluate the filters using cutoff frequencies of 1, 3, and 5 kHz.

TABLE 6: AUROC scores for single-model attribution in an open-world setting using the English ASVspoof LA Benchmark. Each row represents a source: either real audio, samples from various synthesis systems, or samples from the target system itself. Each column corresponds to a target synthesis system. Entries report the AUROC using EnCodec-based residuals, extracted with an STFT window size of 128 and a hop size of 2. Each cell contains two values: correlation-based / Mahalanobis-based attribution scores. Higher AUROC values indicate stronger separation between the target system and all other sources. VC systems are indicated with \*, and systems combining both TTS and VC are marked with ‡. Systems without annotations correspond to TTS-only models.

Source \ Target	A16	A19*
A07	0.78 / 0.71	0.99 / 0.94
A08	0.99 / 1.00	1.00 / 1.00
A09	1.00 / 1.00	1.00 / 1.00
A10	1.00 / 1.00	1.00 / 1.00
A11	1.00 / 1.00	1.00 / 1.00
A12	1.00 / 1.00	1.00 / 1.00
A13‡	1.00 / 1.00	1.00 / 1.00
A14‡	1.00 / 1.00	1.00 / 1.00
A15‡	1.00 / 1.00	1.00 / 1.00
A16	-	0.91 / 0.96
A17*	1.00 / 1.00	1.00 / 1.00
A18*	1.00 / 1.00	1.00 / 0.99
A19*	0.81 / 0.91	-
Bonafide	1.00 / 1.00	1.00 / 1.00
Avg.	<b>0.97 / 0.96</b>	<b>0.99 / 0.99</b>

**Results.** Based on Table 7 a 1 kHz cutoff yields the best overall performance, achieving the highest average AUROC when paired with Mahalanobis scoring (0.96 for A16 and 1.00 for A19). This configuration slightly outperforms the 3 kHz and 5 kHz cutoffs, making it the preferred setting for low-pass filtering-based residuals.

**A.2.2. High-pass filter setup.** This filter isolates higher-frequency content, which may carry artifacts from synthesis systems. We evaluate the filters using cutoff frequencies of 1, 3, and 5 kHz.

**Results.** While Mahalanobis scoring consistently outperforms correlation as reported in Table 8, the overall attribution performance of high-pass filtered residuals is notably lower than that of low-pass filtering (see Table 7).

**A.2.3. Band-stop filter setup.** This filter removes mid-to-high-frequency ranges, useful for testing whether the removed band contains synthesis-specific features. We evaluate the filters with stop bands of 4–7 kHz and 5–6 kHz.

**Results.** As reported in Table 9, the best average AUROC is achieved with the wider 4–7 kHz stop band using Mahalanobis distance (0.90 for A16 and 0.98 for A19), but this still falls short compared to the low-pass configuration with a 1 kHz cutoff, which reached 0.96 and 1.00, respectively.

TABLE 7: Entries report the AUROC using low-pass filtering-based residuals, extracted with an STFT window size of 128 and a hop size of 2 for single-model attribution in an open-world setting using the English ASVspoof LA Benchmark. Each row represents a source: either real audio, samples from various synthesis systems, or samples from the target system itself. Each column corresponds to a target synthesis system. Each cell contains two values: correlation-based / Mahalanobis-based attribution scores. Higher AUROC values indicate stronger separation between the target system and all other sources. Results are grouped by low-pass cutoff frequencies: 1, 3, and 5 kHz. VC systems are indicated with <sup>\*</sup>, and systems combining both TTS and VC are marked with <sup>‡</sup>. Systems without annotations correspond to TTS-only models.

Src \ Tgt	Cutoff = 1 kHz		Cutoff = 3 kHz		Cutoff = 5 kHz	
	A16	A19*	A16	A19*	A16	A19*
A07	0.67 / 0.82	0.97 / 0.99	0.67 / 0.81	0.97 / 0.99	0.63 / 0.78	0.93 / 0.99
A08	0.97 / 1.00	1.00 / 1.00	0.97 / 1.00	1.00 / 1.00	0.95 / 1.00	1.00 / 1.00
A09	0.99 / 1.00	1.00 / 1.00	0.99 / 1.00	1.00 / 1.00	0.99 / 1.00	1.00 / 1.00
A10	0.94 / 1.00	1.00 / 1.00	0.96 / 1.00	1.00 / 1.00	0.96 / 1.00	1.00 / 1.00
A11	0.93 / 1.00	1.00 / 1.00	0.95 / 1.00	1.00 / 1.00	0.96 / 1.00	1.00 / 1.00
A12	0.95 / 1.00	1.00 / 1.00	0.97 / 1.00	1.00 / 1.00	0.98 / 1.00	1.00 / 1.00
A13 <sup>‡</sup>	0.99 / 1.00	1.00 / 1.00	0.99 / 1.00	1.00 / 1.00	0.99 / 1.00	1.00 / 1.00
A14 <sup>‡</sup>	0.98 / 1.00	1.00 / 1.00	0.99 / 1.00	1.00 / 1.00	0.99 / 1.00	1.00 / 1.00
A15 <sup>‡</sup>	0.97 / 1.00	1.00 / 1.00	0.99 / 1.00	1.00 / 1.00	0.98 / 1.00	1.00 / 1.00
A16	-	0.90 / 0.97	-	0.91 / 0.98	- / -	0.87 / 0.98
A17*	0.89 / 1.00	1.00 / 1.00	0.93 / 1.00	1.00 / 1.00	0.96 / 1.00	1.00 / 1.00
A18*	0.48 / 0.99	0.86 / 0.98	0.57 / 0.99	0.89 / 0.97	0.71 / 0.99	0.91 / 0.99
A19*	0.18 / 0.66	-	0.17 / 0.67	-	0.25 / 0.67	-
Bonafide	0.85 / 1.00	0.99 / 1.00	0.89 / 1.00	1.00 / 1.00	0.93 / 1.00	1.00 / 1.00
Avg.	0.84 / <b>0.96</b>	0.98 / <b>1.00</b>	0.86 / <b>0.95</b>	0.98 / <b>0.99</b>	0.87 / <b>0.95</b>	0.97 / <b>0.99</b>

TABLE 8: Entries report the AUROC using high-pass filtering-based residuals, extracted with an STFT window size of 128 and a hop size of 2 for single-model attribution in an open-world setting using the English ASVspoof LA Benchmark. Each row represents a source: either real audio, samples from various synthesis systems, or samples from the target system itself. Each column corresponds to a target synthesis system. Each cell contains two values: correlation-based / Mahalanobis-based attribution scores. Higher AUROC values indicate stronger separation between the target system and all other sources. Results are grouped by high-pass cutoff frequencies: 1, 3, and 5 kHz. VC systems are indicated with <sup>\*</sup>, and systems combining both TTS and VC are marked with <sup>‡</sup>. Systems without annotations correspond to TTS-only models.

Src \ Trg	Cutoff = 1 kHz		Cutoff = 3 kHz		Cutoff = 5 kHz	
	A16	A19*	A16	A19*	A16	A19*
A07	0.69 / 0.68	0.96 / 0.98	0.70 / 0.71	0.83 / 0.97	0.75 / 0.75	0.86 / 0.97
A08	0.70 / 0.97	0.96 / 1.00	0.92 / 0.97	0.97 / 1.00	0.92 / 0.99	0.92 / 1.00
A09	0.91 / 0.95	0.99 / 1.00	0.85 / 0.94	0.95 / 1.00	0.70 / 0.97	0.79 / 1.00
A10	0.63 / 0.87	0.94 / 1.00	0.72 / 0.93	0.85 / 0.99	0.72 / 0.96	0.85 / 1.00
A11	0.66 / 0.84	0.95 / 1.00	0.74 / 0.94	0.85 / 1.00	0.74 / 0.97	0.86 / 1.00
A12	0.60 / 0.82	0.88 / 1.00	0.63 / 0.89	0.76 / 1.00	0.53 / 0.96	0.71 / 1.00
A13 <sup>‡</sup>	0.76 / 0.90	0.98 / 1.00	0.80 / 0.96	0.91 / 1.00	0.80 / 0.98	0.89 / 1.00
A14 <sup>‡</sup>	0.78 / 0.86	0.98 / 1.00	0.81 / 0.96	0.92 / 1.00	0.73 / 0.98	0.82 / 1.00
A15 <sup>‡</sup>	0.62 / 0.79	0.96 / 1.00	0.58 / 0.87	0.78 / 0.99	0.53 / 0.95	0.64 / 0.99
A16	-	0.79 / 0.98	-	0.70 / 0.98	-	0.64 / 0.97
A17*	0.35 / 0.80	0.70 / 0.96	0.39 / 0.85	0.46 / 0.94	0.41 / 0.94	0.46 / 0.97
A18*	0.53 / 0.59	0.47 / 0.88	0.41 / 0.68	0.48 / 0.89	0.36 / 0.78	0.50 / 0.95
A19*	0.60 / 0.55	-	0.42 / 0.52	-	0.43 / 0.60	-
Bonafide	0.49 / 0.77	0.53 / 0.95	0.57 / 0.85	0.66 / 0.95	0.61 / 0.93	0.64 / 0.97
Avg.	0.67 / <b>0.81</b>	0.84 / <b>0.98</b>	0.66 / <b>0.85</b>	0.78 / <b>0.98</b>	0.63 / <b>0.91</b>	0.73 / <b>0.98</b>

**A.2.4. Band-pass filter.** In contrast to band-stop, these preserve only the selected frequency band, allowing analysis of

TABLE 9: Entries report the AUROC using band-stop filtering-based residuals, extracted with an STFT window size of 128 and a hop size of 2 for single-model attribution in an open-world setting using the English ASVspoof LA Benchmark. Each row represents a source: either real audio, samples from various synthesis systems, or samples from the target system itself. Each column corresponds to a target synthesis system. Each cell contains two values: correlation-based / Mahalanobis-based attribution scores. Higher AUROC values indicate stronger separation between the target system and all other sources. Results are grouped by a band-stop filter with a stop band of: 4–7 kHz and 5–6 kHz. VC systems are indicated with <sup>\*</sup>, and systems combining both TTS and VC are marked with <sup>‡</sup>. Systems without annotations correspond to TTS-only models.

Src \ Tgt	Stop band = 4–7 kHz		Stop band = 5–6 kHz	
	A16	A19*	A16	A19*
A07	0.59 / 0.74	0.82 / 0.97	0.52 / 0.67	0.67 / 0.95
A08	0.77 / 0.99	0.96 / 1.00	0.80 / 0.98	0.91 / 1.00
A09	0.70 / 0.97	0.93 / 1.00	0.44 / 0.94	0.73 / 1.00
A10	0.60 / 0.92	0.82 / 1.00	0.49 / 0.88	0.66 / 0.99
A11	0.61 / 0.96	0.84 / 1.00	0.61 / 0.91	0.77 / 1.00
A12	0.51 / 0.95	0.82 / 1.00	0.46 / 0.93	0.75 / 1.00
A13 <sup>‡</sup>	0.68 / 0.97	0.88 / 1.00	0.57 / 0.95	0.71 / 1.00
A14 <sup>‡</sup>	0.61 / 0.96	0.88 / 1.00	0.43 / 0.92	0.70 / 1.00
A15 <sup>‡</sup>	0.50 / 0.95	0.81 / 1.00	0.46 / 0.91	0.64 / 1.00
A16	-	0.80 / 0.97	-	0.72 / 0.96
A17*	0.37 / 0.96	0.54 / 0.99	0.51 / 0.92	0.54 / 0.99
A18*	0.49 / 0.79	0.48 / 0.83	0.38 / 0.61	0.36 / 0.71
A19*	0.38 / 0.59	-	0.57 / 0.51	-
Bonafide	0.38 / 0.95	0.61 / 0.99	0.51 / 0.89	0.54 / 0.98
Avg.	0.55 / <b>0.90</b>	0.79 / <b>0.98</b>	0.50 / <b>0.85</b>	0.68 / <b>0.97</b>

synthesis artifacts isolated to mid-high ranges. We evaluate band-pass filters with pass bands of 4–7 kHz and 5–6 kHz.

**Results.** Based on Table 10, these results are on par with those obtained using low-pass filtered residuals, demonstrating that attribution signals are also strongly expressed within these mid-frequency bands. Although the main paper adopts low-pass filtering as the winner configuration, this band-pass variant emerges as a strong candidate and merits further exploration.

## Appendix B. Baseline Model Architectures

We describe the network architectures, preprocessing methods, and relevant training details for reproducibility and clarity.

**X-vector.** We adopt a time-delay neural network (TDNN)-based X-vector model [63], [64], originally introduced by Snyder et al. [59]. The model consists of five TDNN layers with context sizes {5, 3, 2, 1, 1} and dilations {1, 1, 2, 1, 3}, each followed by ReLU activation and dropout ( $p = 0.5$ ). Statistical pooling (mean and standard deviation) is ap-

TABLE 10: Entries report the AUROC using band-pass filtering-based residuals, extracted with an STFT window size of 128 and a hop size of 2 for single-model attribution in an open-world setting using the English ASVspoof LA Benchmark. Each row represents a source: either real audio, samples from various synthesis systems, or samples from the target system itself. Each column corresponds to a target synthesis system. Each cell contains two values: correlation-based / Mahalanobis-based attribution scores. Higher AUROC values indicate stronger separation between the target system and all other sources. Results are grouped by a band-pass filter with a band pass of: 4–7 kHz and 5–6 kHz. VC systems are indicated with <sup>\*</sup>, and systems combining both TTS and VC are marked with <sup>‡</sup>. Systems without annotations correspond to TTS-only models.

Src \ Tgt	Pass band = 4–7 kHz		Pass band = 5–6 kHz	
	A16	A19*	A16	A19*
A07	0.64 / 0.78	0.89 / 0.98	0.62 / 0.76	0.89 / 0.98
A08	0.90 / 1.00	0.98 / 1.00	0.91 / 1.00	0.99 / 1.00
A09	0.98 / 1.00	1.00 / 1.00	0.97 / 1.00	1.00 / 1.00
A10	0.97 / 1.00	0.99 / 1.00	0.95 / 1.00	0.99 / 1.00
A11	0.97 / 1.00	0.99 / 1.00	0.94 / 1.00	0.98 / 1.00
A12	0.99 / 1.00	1.00 / 1.00	0.97 / 1.00	0.99 / 1.00
A13 <sup>‡</sup>	1.00 / 1.00	1.00 / 1.00	0.99 / 1.00	1.00 / 1.00
A14 <sup>‡</sup>	1.00 / 1.00	1.00 / 1.00	0.99 / 1.00	1.00 / 1.00
A15 <sup>‡</sup>	0.99 / 1.00	0.99 / 1.00	0.98 / 1.00	1.00 / 1.00
A16	-	0.84 / 0.98	-	0.83 / 0.98
A17*	0.98 / 1.00	0.99 / 1.00	0.95 / 1.00	0.98 / 1.00
A18*	0.88 / 1.00	0.92 / 0.99	0.80 / 1.00	0.86 / 0.98
A19*	0.34 / 0.64	-	0.35 / 0.64	-
Bonafide	0.96 / 1.00	0.99 / 1.00	0.92 / 1.00	0.98 / 1.00
Avg.	0.88 / <b>0.95</b>	0.97 / <b>1.00</b>	0.88 / <b>0.97</b>	0.97 / <b>0.99</b>

plied over the time dimension to produce a fixed 1,024-dimensional embedding, which is passed through a two-layer multi-layer perceptron (MLP) with 512 units per layer and finally mapped to class logits via a softmax output layer.

**LCNN.** We implement a Light Convolutional Neural Network (LCNN) following the design of Lavrentyeva et al. [60], which incorporates the Max-Feature-Map (MFM) activation [65]. The model consists of nine convolutional blocks with interleaved MFM activations and batch normalization. Selected blocks are followed by max-pooling for spatial downsampling. An adaptive max-pooling layer aggregates spatial features into a fixed-length vector, which is processed by a two-layer MLP with dropout ( $p = 0.75$ ), batch normalization, and MFM activation. A softmax output layer produces class logits.

**ResNet.** We implement a ResNet-18 [61] architecture, composed of four residual stages with 2, 2, 2, and 2 blocks respectively. Each block contains two  $3 \times 3$  convolutions with batch normalization and ReLU, and includes skip connections with optional downsampling. The network begins with a  $7 \times 7$  convolution (stride 2), followed by batch normalization, ReLU, and max-pooling. After the residual stages, global average pooling generates a fixed-size feature vector, which is passed to a single MLP head for classification.

**SE-ResNet.** We extend the ResNet-18 architecture by integrating Squeeze-and-Excitation (SE) blocks [62] into each residual block. Each SE module applies global average pooling followed by a two-layer MLP (with ReLU and sigmoid activations) to compute channel-wise scaling factors. These are used to reweight feature maps before the residual addition. The overall architecture mirrors that of ResNet-18, with downsampling performed via strided convolutions in the first block of each stage. The final global average pooled feature vector is fed into a classification MLP.

**VFD-Net.** We implement a ResNet-18-based architecture adapted from Deng et al. [13], modified to accept 16-channel input features. After standard ResNet layers and four residual stages ( $\{64, 128, 256, 512\}$  channels), global average pooling produces a 512-dimensional feature vector. Two heads follow: (1) a classification head using a single fully connected layer, and (2) a projection head, which is a two-layer MLP (128 hidden units, 64 output), using ReLU activation and  $\ell_2$  normalization for contrastive learning. Training uses a multi-task loss combining cross-entropy and supervised contrastive loss [66], with weighting learned via the uncertainty-based method [67].

Depending on the baseline model, different time-frequency representations are applied as inputs:

- ResNet, SE-ResNet, LCNN, and X-vector: These models receive linear frequency cepstral coefficients (LFCCs) as input. LFCCs are extracted using 20 filters and 60 coefficients, with an STFT configured for a window length of 25 ms and a hop length of 10 ms. A Hann window function is applied.
- VFD-Net: This model uses log-mel spectrograms with 80 mel bands, computed using an STFT with a 1200-sample window and 300-sample hop. A Hamming window function is applied.